White Rose Research Online

eprints@whiterose.ac.uk
https://eprints.whiterose.ac.uk
Universities of Leeds, Sheffield and York

Deposited via The University of Leeds.

White Rose Research Online URL for this paper:
https://eprints.whiterose.ac.uk/id/eprint/81538/

Version: Accepted Version

Article:
Smith, CJ, Forster, PM and Crook, R (2014) Global analysis of photovoltaic energy output enhanced by phase change material cooling. Applied Energy, 126. 21 - 28. ISSN: 0306-2619

https://doi.org/10.1016/j.apenergy.2014.03.083

Reuse
Items deposited in White Rose Research Online are protected by copyright, with all rights reserved unless indicated otherwise. They may be downloaded and/or printed for private study, or other acts as permitted by national copyright laws. The publisher or other rights holders may allow further reproduction and re-use of the full text version. This is indicated by the licence information on the White Rose Research Online record for the item.

Takedown
If you consider content in White Rose Research Online to be in breach of UK law, please notify us by emailing eprints@whiterose.ac.uk including the URL of the record and the reason for the withdrawal request.

UNIVERSITY OF LEEDS
University of Sheffield
UNIVERSITY of York

Global analysis of photovoltaic energy output enhanced by phase change material cooling

Christopher J. Smith[a,*], Piers M. Forster[b], Rolf Crook[a]

[a] *Energy Research Institute, University of Leeds, Leeds, LS2 9JT, United Kingdom*
[b] *School of Earth and Environment, University of Leeds, Leeds, LS2 9JT, United Kingdom*

Abstract

This paper describes a global analysis to determine the increase in annual energy output attained by a PV system with an integrated phase change material (PCM) layer. The PCM acts as a heat sink and limits the peak temperature of the PV cell thereby increasing efficiency. The simulation uses a one-dimensional energy balance model with ambient temperature, irradiance and wind speed extracted from ERA-Interim reanalysis climate data over a 1.5° longitude × 1.5° latitude global grid. The effect of varying the PCM melting temperature from 0°C to 50°C was investigated to identify the optimal melting temperature at each grid location. PCM-enhanced cooling is most beneficial in regions with high insolation and little intra-annual variability in climate. When using the optimal PCM melting temperature, the annual PV energy output increases by over 6% in Mexico and eastern Africa, and over 5% in many locations such as Central and South America, much of Africa, Arabia, Southern Asia and the Indonesian archipelago. In Europe, the energy output enhancement varies between 2% and nearly 5%. In general, high average ambient temperatures correlate with higher optimal PCM melting temperatures. The sensitivity to PCM melting temperature was further investigated at locations where large solar PV arrays currently exist or are planned to be constructed. Significant improvements in performance are possible even when a sub-optimal PCM melting temperature is used. A brief economic assessment based on typical material costs and energy prices shows that PCM cooling is not currently cost-effective for single-junction PV.

Keywords: Phase change material, photovoltaics, global study, heat transfer, simulation

1. Introduction

The addition of phase change material (PCM) to a solar cell has been proposed as a method to increase solar PV energy output by keeping the temperature of PV cells close to the ambient [1]. The PCM is a layer of high latent heat capactiy which acts as a heat sink, absorbing heat that is transferred from a PV cell. Solar cell efficiency is dependent on cell temperature, with a drop in efficiency of 0.45% (relative) for every 1°C rise in cell temperature for crystalline silicon [2]. Therefore, any mechanism which reduces the cell temperature, particularly at times of high irradiance, will increase cell efficiency and PV energy output. Alongside phase change materials, existing cooling methods proposed include water and air cooling. Water cooling may be unsuitable due to the weight of water required to deliver appropriate cooling [3]; furthermore, in many locations where solar energy has great potential such as deserts, water is scarce. If either air or water cooling is activated, this introduces a maintanence burden that could increase operating costs and system downtime.

The potential for improvement by using a PV/PCM system has been demonstrated in numerical simulations [1, 4], laboratory tests [1, 5, 6] and in outdoor studies [5, 7, 8]. In terms of outdoor testing of PV/PCM systems, it was estimated that efficiency from a PV/PCM system would be improved by 7.5% at peak solar hours due to a 17°C difference in temperature between an aluminium flat plate and an aluminium box containing PCM [5]. A PV/PCM panel tested outdoors in Pakistan resulted in a PV cell temperature that was 21.5°C lower than the reference at the peak time of the day [7]. These figures are maximum temperature differentials as the PCM and non-PCM systems change temperature at different rates due to the difference in thermal masses. However over the course of the day it was calculated that PV energy output would be improved by 6.8% compared the reference cell, estimated from the cell manufacturers' data of a 0.5% K^{-1} decline in efficiency and the temperature difference between the cells at each point during the day. In the cooler climate of Ireland in mid-September, the power output increase was approximately 3.8% with the same PCM. During an experiment in Western India it was demonstrated that PCM cooling could be very promising for use in concentrating solar PV cells [8].

This paper evaluates the global potential for PCM-assisted cooling by measuring the absolute and relative increases in electrical output from a silicon solar cell using a numerical simulation. The simulation is performed globally using typical climatological data for each region. For sites of current and future interest for solar PV, the dependence in energy output on PCM melting temperature is analysed. The locations where PCM-assisted cooling is likely to lead to significant energy output increases are therefore identified.

*Corresponding author
Email address: pmcjs@leeds.ac.uk (Christopher J. Smith)

2. Model PV/PCM cell

The model PV/PCM cell consists of a solar cell layered on top of an aluminium box containing PCM (Fig. 1). The heat transfer through a PV/PCM cell is modelled performed using a one dimensional finite difference energy balance method with a one hour timestep. The energy balance scheme consists of the incoming solar energy less the heat lost to the surroundings in the form of convection and radiation and energy extracted in the form of electricity (Fig. 1). Conductive heat exchange occurs between each component of the PV/PCM cell.

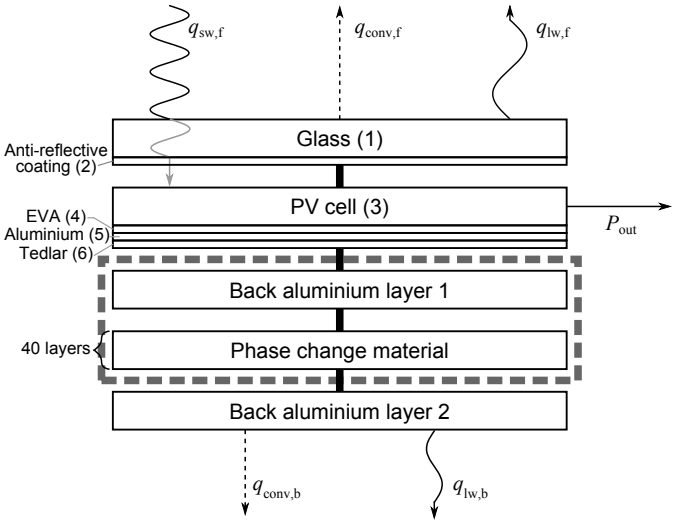

Figure 1: Energy balance diagram showing the energy fluxes into and out of the PV/PCM system. The thick black lines represent conductive heat exchange. Subscripts are defined as follows: sw = shortwave, lw = longwave, conv = convective, f = front, b = back. P_{out} is the electrical energy generated by the cell. The dotted grey box encompasses the components of the PV/PCM system that are omitted from the reference PV system. Numbers in brackets refer to the subscripts given to each layer in Table 1 and eqs. (1) to (6).

2.1. PV cell

The PV cell is based on that of Armstrong and Hurley [9] and has 6 separate layers numbered 1–6 in Fig. 1 and Table 1. Given the small heat capacity of the some of the layers, the glass and anti-reflective coating are treated as one combined thermal mass, referred to hereafter as the *glass* layer, and the PV cell, EVA layer, aluminium rear contact and Tedlar backing are combined into another separate thermal mass, referred to hereafter as the *cell* layer. The combining of small thermal masses improves the numerical stability of the model by avoiding division by very small numbers.

The total heat capacity (J K^{-1}) of the glass layer is given by

$$C_{\text{glass}} = A\left(\rho_1 c_{p1} z_1 + \rho_2 c_{p2} z_2\right) \quad (1)$$

and thermal conductance (W K^{-1}) is given by

$$G_{\text{glass}} = \frac{A}{z_1/k_1 + z_2/k_2} \quad (2)$$

where A is the area of the cell. The heat capacity and thermal conductance of the PV cell layer is similarly given by

$$C_{\text{cell}} = A\left(\rho_3 c_{p3} z_3 + \rho_4 c_{p4} z_4 + \rho_5 c_{p5} z_5 + \rho_6 c_{p6} z_6\right) \quad (3)$$

and

$$G_{\text{cell}} = \frac{A}{z_3/k_3 + z_4/k_4 + z_5/k_5 + z_6/k_6}. \quad (4)$$

2.2. Aluminium casing

The PV cell described is attached to an aluminium box which sandwiches the PCM following the experimental methods of Huang *et al.* [5]. It was shown that a highly conductive material for the PCM housing such as aluminium is more effective than an insulating housing such as Perspex [10]. Heat losses through the sides of the PCM box are assumed to be negligible compared to the front and back of the box based on a cell size of $A = 1$ m^2.

Both top and bottom aluminium sheets have heat capacity and thermal conductance G_{alu} given by

$$C_{\text{alu}} = A\rho_{\text{alu}} c_{p,\text{alu}} z_{\text{alu}} \quad (5)$$

and

$$G_{\text{alu}} = \frac{A k_{\text{alu}}}{z_{\text{alu}}}. \quad (6)$$

with $z_{\text{alu}} = 5$ mm and values of ρ, c_p and k the same as for the back-contact aluminium given in Table 1.

2.3. Phase change material

PCMs can either be isothermal or undergo a small phase change temperature range. Various materials have been exploited as PCMs, including salt hydrates, fatty acids and paraffin waxes [11]. Paraffin waxes attain their highly tunable melting points due to the varying chain lengths of their constituent hydrocarbons, and as such experience a phase change range [12].

Ideally, a PCM should have a small thermal expansion coefficient, high thermal conductivity, high latent heat of fusion and a high specific heat capacity [4]. The thermal expansion of the PCM is assumed to be small [13]. PCMs available commercially tend to have low coefficients of thermal conductivity, which limits the rate of heat transfer [14]. However, thermal conductivity can be improved in several ways. Examples of this include metal fins attached to the PCM aluminium layer which increase the contact surface area between the plate and PCM, inserting a metal mesh into the PCM, inserting high thermal conductivity particles into the PCM, micro-encapsulation of the PCM, or metal conductive strips interspersed within the PCM [8, 15]. Enhancements in thermal conductance by a factor of 10–20 over a plain PCM layer have been reported [16]. In this study, a heat transfer enhancement factor of 2 is used.

The PCM component is thick and has a low thermal conductance compared to the PV and aluminium components. Therefore the PCM has been divided into 40 layers to model the temperature gradient through the PCM. In liquid regions of the PCM, flow is assumed to be laminar and heat transfer primarily occurs by conduction rather than convection, an assumption

Subscript	Layer	ρ	c_p	z	k
1	Glass covering	3000	500	0.003	1.8
2	Anti-reflective coating	2400	691	1.0×10^{-7}	32
3	PV cells	2330	677	2.25×10^{-4}	148
4	EVA	960	2090	5.0×10^{-4}	0.35
5	Aluminium (cell)	2700	900	1.0×10^{-5}	237
6	Tedlar	1200	1250	0.0001	0.2

Table 1: Heat transfer parameters of the PV panel, from references within [9]. ρ: material density (kg m^{-3}), c_p: specific heat capacity (J kg^{-1} K^{-1}), z: material thickness (m), k: thermal conductivity (W m^{-1} K^{-1}).

validated by other models [7]. This enables a one-dimensional numerical model to be used where PCM temperature is a function of depth only. The properties of the PCM are shown in Table 2.

The heat content of a non-isothermal PCM can be modelled using the enthalpy method or the effective heat capacity method [13]. The enthalpy method describes the total heat content of the PCM as a monotonically increasing, continuous and invertible function of temperature. Based on paraffin wax PCM melting profiles in the literature [13, 17] the enthalpy function of the PCM can be described to a good approximation by a hyperbolic tangent model:

$$\begin{aligned} H = \frac{1}{2}\Big[&C_{\mathrm{pcms}}T_{\mathrm{pcm}}(1-\tanh(s(T_{\mathrm{pcm}}-T_{\mathrm{melt}}))) \\ &+ Q_{\mathrm{liq}}(1+\tanh(s(T_{\mathrm{pcm}}-T_{\mathrm{melt}}))) \\ &+ C_{\mathrm{pcml}}(T_{\mathrm{pcm}}-T_{\mathrm{melt}})(1+\tanh(s(T_{\mathrm{pcm}}-T_{\mathrm{melt}})))\Big] \end{aligned} \quad (7)$$

where s is a scale factor that describes the steepness of the phase change region of the curve. $s = \infty$ for an isothermal PCM. The effective heat capacity of the PCM layer is given by the derivative of enthalpy with respect to T_{pcm} [18]. In Eq. (7), the cumulative heat required to melt the PCM is given by

$$Q_{\mathrm{liq}} = \frac{Az_{\mathrm{pcm}}}{l}\left(\rho_{\mathrm{pcms}}c_{\mathrm{pcms}}T_{\mathrm{melt}} + \rho_{\mathrm{pcml}}L\right) \quad (8)$$

and the solid and liquid heat capacities C_{pcms} and C_{pcml} respectively of each layer are

$$C_{\mathrm{pcm}} = Ac_{\mathrm{pcm}}\rho_{\mathrm{pcm}}\frac{z_{\mathrm{pcm}}}{l} \quad (9)$$

where the parameters for solid or liquid PCM from Table 2 are used in Eq. (9) as appropriate. The thermal conductance of each PCM layer $j = 1, \ldots, 40$ is given by the proportion of solid and liquid PCM in each layer which follows from the enthalpy function:

$$G_{\mathrm{pcm}j} = \frac{G_{\mathrm{pcml}} - G_{\mathrm{pcms}}}{2}(1+\tanh(s(T_{\mathrm{pcm}j}-T_{\mathrm{melt}}))) + G_{\mathrm{pcms}} \quad (10)$$

where the thermal conductance of solid (G_{pcms}) and liquid (G_{pcml}) PCM is

$$G_{\mathrm{pcm}} = \frac{Apk_{\mathrm{pcm}}}{z_{\mathrm{pcm}}/l}. \quad (11)$$

3. Energy balance scheme

3.1. Meteorological data

Synoptic monthly means of the 2 m air temperature, 10 m eastward and northward wind components and surface solar radiation downwards were taken from ERA-Interim reanalysis data [19] with a global resolution of 1.5° longitude × 1.5° latitude. The 12-month period spanning July 2012 to June 2013 was used as the meteorological year under consideration and the reanalysis data provides even global spatial coverage from a combination of observations, numerical weather models and forecasts [20].

Monthly mean synoptic data is available 8 times per day from 0000 UTC in 3-hour steps. The surface solar radiation downwards field gives integrated global horizontal irradiance totals in 3-hour steps for the half-days ending at 0000 UTC and 1200 UTC. To recover the insolation for each 3-hour period, the difference between the irradiation values at the start and the end of each 3-hour time period was taken and this total divided by 10800 seconds to convert from a total irradiation to an average insolation. The insolations derived were deemed to be the irradiance values at the midpoint of each 3-hour period (i.e. at times 0130 UTC, 0430 UTC, and so on). The magnitude of the 10 m wind speed is given as $W = \sqrt{U^2 + V^2}$ where U and V are the eastward and northward wind components respectively. From the 3-hour irradiance, temperature and wind speed data, hourly values of each variable were extracted using cubic spline interpolation.

3.2. Numerical model

The energy balance through the PV/PCM system is modelled as a system of 44 simultaneous differential equations. The change in temperature in each layer is governed by

$$\begin{aligned} \frac{\mathrm{d}T_{\mathrm{glass}}}{\mathrm{d}t} = \frac{1}{C_{\mathrm{glass}}}\big[&q_{\mathrm{sw,f}} + q_{\mathrm{lw,f}} + q_{\mathrm{conv,f}} + \\ &G_{\mathrm{glass}}(T_{\mathrm{cell}} - T_{\mathrm{glass}})\big] \end{aligned} \quad (12)$$

$$\begin{aligned} \frac{\mathrm{d}T_{\mathrm{cell}}}{\mathrm{d}t} = \frac{1}{C_{\mathrm{cell}}}\big[&G_{\mathrm{cell}}(T_{\mathrm{alu1}} + T_{\mathrm{glass}} - 2T_{\mathrm{cell}}) + \\ &A\alpha_{\mathrm{cell}}\tau_{\mathrm{cell}}(1-\alpha_{\mathrm{glass}})I - P_{\mathrm{out}}\big] \end{aligned} \quad (13)$$

$$\frac{\mathrm{d}T_{\mathrm{alu1}}}{\mathrm{d}t} = \frac{1}{C_{\mathrm{alu}}}\left[G_{\mathrm{alu}}(T_{\mathrm{pcm1}} + T_{\mathrm{cell}} - 2T_{\mathrm{alu1}})\right] \quad (14)$$

Parameter	Symbol	Value
Specific heat capacity of PCM, solid	c_{pcms}	2900 J kg^{-1} K^{-1} [4]
Specific heat capacity of PCM, liquid	c_{pcml}	2100 J kg^{-1} K^{-1} [4]
Latent heat of PCM	L	2.1×10^5 J kg^{-1} [4]
Density of PCM, solid	ρ_{pcms}	860 kg m^{-3} [4]
Density of PCM, liquid	ρ_{pcml}	780 kg m^{-3} [4]
Thickness of PCM	z_{pcm}	0.05 m
Thermal conductivity of PCM, solid	k_{pcms}	0.24 W m^{-1} K^{-1} [4]
Thermal conductivity of PCM, liquid	k_{pcml}	0.15 W m^{-1} K^{-1} [4]
PCM layers	l	40
PCM melting temperature	T_{melt}	5–60°C in 1°C intervals
PCM conductance enhancement	p	2 [4]

Table 2: Properties of the phase change material used in this study

$$\frac{\mathrm{d}T_{\mathrm{pcm1}}}{\mathrm{d}t} = \frac{1}{\mathrm{d}H/\,\mathrm{d}T_{\mathrm{pcm1}}}[G_{\mathrm{pcm1}}(T_{\mathrm{pcm2}} + T_{\mathrm{alu1}} - 2T_{\mathrm{pcm1}})] \quad (15)$$

$$\frac{\mathrm{d}T_{\mathrm{pcm}j}}{\mathrm{d}t} = \frac{1}{\mathrm{d}H/\,\mathrm{d}T_{\mathrm{pcm}j}}\Big[G_{\mathrm{pcm}j}(T_{\mathrm{pcm}(j+1)} + T_{\mathrm{pcm}(j-1)} - 2T_{\mathrm{pcm}j})\Big], \qquad j = 2, \ldots, 39 \quad (16)$$

$$\frac{\mathrm{d}T_{\mathrm{pcm40}}}{\mathrm{d}t} = \frac{1}{\mathrm{d}H/\,\mathrm{d}T_{\mathrm{pcm40}}}\Big[G_{\mathrm{pcm40}}(T_{\mathrm{alu2}} + T_{\mathrm{pcm39}} - 2T_{\mathrm{pcm40}})\Big] \quad (17)$$

$$\frac{\mathrm{d}T_{\mathrm{alu2}}}{\mathrm{d}t} = \frac{1}{C_{\mathrm{alu}}}\Big[G_{\mathrm{alu}}(T_{\mathrm{pcm40}} - T_{\mathrm{alu2}}) + q_{\mathrm{lw,b}} + q_{\mathrm{conv,b}}\Big] \quad (18)$$

where T_i is the temperature of each layer, alu1 and alu2 refer to the front and back aluminium sheets, and t is time.

The reference system differs from the PV/PCM system in that T_{alu1} in Eq. (13) becomes T_{alu}, Eqs. (14)–(17) are omitted and Eq. (18) is modified to become

$$\frac{\mathrm{d}T_{\mathrm{alu2}}}{\mathrm{d}t} = \frac{1}{C_{\mathrm{alu}}}\left[G_{\mathrm{alu}}(T_{\mathrm{cell}} - T_{\mathrm{alu}}) + q_{\mathrm{lw,b}} + q_{\mathrm{conv,b}}\right]. \quad (19)$$

The change in nomenclature from alu2 to alu highlights the fact there is only one aluminium sheet in the reference system. The heat flows between the PV systems and the ambient are given by

$$q_{\mathrm{sw,f}} = A\alpha_{\mathrm{glass}}I \quad (20)$$

$$q_{\mathrm{lw,f}} = A\sigma(\epsilon_{\mathrm{sky}}T_{\mathrm{sky}}^4 - \epsilon_{\mathrm{glass}}T_{\mathrm{glass}}^4) \quad (21)$$

$$q_{\mathrm{conv,f}} = Ah_{\mathrm{air}}(T_{\mathrm{air}} - T_{\mathrm{glass}}) \quad (22)$$

$$q_{\mathrm{lw,b}} = A\sigma(\epsilon_{\mathrm{ground}}T_{\mathrm{ground}}^4 - \epsilon_{\mathrm{alu}}T_{\mathrm{alu}(2)}^4) \quad (23)$$

$$q_{\mathrm{conv,b}} = Ah_{\mathrm{air}}(T_{\mathrm{air}} - T_{\mathrm{alu}(2)}) \quad (24)$$

$$P_{\mathrm{out}} = A\eta I \quad (25)$$

with I the solar irradiance in W m^{-2} and T_{air} the ambient temperature. It is assumed that $T_{\mathrm{ground}} = T_{\mathrm{air}}$ [21]. The sky temperature is described by the relationship of Swinbank [22]:

$$T_{\mathrm{sky}} = 0.0552T_{\mathrm{air}}^{1.5}. \quad (26)$$

For the windward (top) face of the PV panel, forced convection due to the wind will dominate free convection. The empirical heat transfer coefficient of Loveday and Taki [23] is used:

$$h_{\mathrm{air}} = 8.91 + 2.00W \quad (27)$$

which is valid for wind speeds W up to 15 m s^{-1}. The cell is assumed to be configured on an open mount and as such the coefficient of convective transfer is assumed to be the same on the reverse side of the panel.

The efficiency of the PV cell η is a function of ambient temperature and irradiance [24] such that

$$\eta = \eta_{\mathrm{ref}}\left[1 - \beta\,(T_{\mathrm{cell}} - 25) + \gamma \log_{10}(I/1000)\right]. \quad (28)$$

In Eq. (28), β is the decline in cell efficiency with respect to temperature of 0.0045 K^{-1}, and $\gamma = 0.1$ is the adjustment in efficiency to account for performance decline in low light conditions. η_{ref} is a reference efficiency of 15.6% at a cell temperature of 25°C and an irradiance level of 1000 W m^{-2}. Other parameters relevant to the PV cell energy balance scheme used in Eqs. (12)–(28) are given in Table 3.

The initial conditions for the temperature of each layer of the PV cell were taken from the Nominal Operating Cell Temperature (NOCT) formula [26], which provides a good first approximation to cell temperature:

$$T_{\mathrm{cell}} = T_{\mathrm{air}} + \frac{T_{\mathrm{NOCT}} - 20}{800}I \quad (29)$$

with $T_{\mathrm{NOCT}} = 45$°C. The model was run from local midnight in each location in order to give the model time to spin up with no solar irradiance input, therefore except in polar summer the initial condition for cell temperature is that it is equal to air temperature.

3.3. Cell temperature under PV/PCM model

The temperatures of a solar cell from both a PV/PCM system and a reference system are shown for an example location in a Northern European summer in Fig. 2a. The addition of the PCM layer causes a delay in temperature rise compared to the reference cell before the PCM has commenced melting because of the additional thermal mass in the system which absorbs heat from the PV cell layer. When the PCM begins to

Parameter	Symbol	Value
Area of PV panel	A	1 m^2
Absorptance of glass	α_{glass}	0.05
Absorptance of cell	α_{cell}	0.9 [21]
Transmissivity of glass	τ_{glass}	0.95 [21]
Stefan-Boltzmann constant	σ	5.67×10^{-8} W m^{-2} K^{-4}
Emissivity of the sky	ϵ_{sky}	0.95 [25]
Emissivity of glass	ϵ_{glass}	0.95
Emissivity of the ground	ϵ_{ground}	0.95 [25]
Emissivity of back layer	ϵ_{alu}	0.02

Table 3: Parameters used within this study to simulate the energy balance through the PV cell.

reach the melting temperature, thermal energy is absorbed by the PCM as it starts to melt, which further slows down the rate of temperature increase in the PV cell. Peak temperature in the PV/PCM cell is reached later than peak temperature in the reference cell. The larger thermal mass of the PV/PCM cell results in it cooling more slowly than the reference cell after reaching peak temperature, and as it approaches the phase change range from above thermal energy is returned from the PCM to the solar cell causing the cell to remain warmer than the reference cell. By the time of day that the PV/PCM cell is warmer than the reference, irradiance levels are low and the PV panel generates only a small fraction of its total daily electricity output. This is expected, in line with previous outdoor experiments [5]. The effect is displayed in Fig. 2b, where it is shown that the gain in power from the PV/PCM cell compared to the reference cell during the middle of the day more than offsets the marginal negative contribution in the early morning and late afternoon when irradiance levels are much lower than at midday. Through the evening, the PV/PCM cell is significantly warmer than the reference cell as the PCM layer continues to dispose of its heat.

4. Results of global simulation

Energy output was calculated for all land points on a 1.5° × 1.5° grid excluding the Antarctic continent. The total annual energy output at each grid point, in kWh, is given by

$$E = \frac{365}{12000} \sum_{m=1}^{12} \sum_{h=0}^{23} I_{hm} \eta_{hm}. \qquad (30)$$

Irradiance and solar cell efficiency are sampled hourly, and the sum runs over the hours of each typical day h and months of the year m. The factor of 365/12 is to scale the one day per month result to a full year and the additional factor of 1/1000 converts from Wh to kWh.

4.1. Annual increase in energy output

Figs. 3a and 3b show the insolation and annual average temperature from the ERA reanalysis data. The power output for each grid point was calculated both under the reference PV panel and the PV/PCM system for PCM melting temperatures varying between 0–50°C in 1°C intervals, and the PCM melting temperature that produced the largest gain in energy output at each grid point was found (Fig. 3c). The general trend is for regions that experience the highest ambient temperatures to benefit from the higher PCM melting temperatures, with the optimal melting temperature in excess of 30°C for much of Africa, the Middle East, South Asia, Australia, and South America. There are several notable high-insolation areas where low PCM melting temperatures are favoured such as the region North East of the Himalayas and in the mountain ranges on the West coast of South America. Regions which are typically cool and do not receive high irradiance levels show a preference for lower PCM melting temperatures.

The largest relative improvements from PV/PCM systems over non-PCM systems are located in Africa, the Middle East, Central and South America, and the Indonesian archipelago (Fig. 3d). An improvement in energy output of over 6% is seen on the Western coast of Mexico and improvements of over 5% are seen in many regions. These highly suitable locations for PCM are all characterised by high ambient temperatures, except for on the West coast of South America. In all other parts of the world, although the relative improvement tends to be lower, there is still a positive increase in electrical energy output to be gained from using a PCM with the optimal melting temperature for the location.

The greatest absolute energy increase using a PCM is again to be found in tropical regions and is mostly coincident with the locations of relative improvement as shown in Fig. 3e, with parts of the Sahara, Central America, Chile and the Arabian peninsula showing an annual electrical output increase of over 20 kWh m^{-2}.

4.2. Sensitivity of energy output increase to PCM melting temperature

Locations that are geographically varied and where large solar farms either currently exist or are planned to be built were investigated further to determine sensitivity to PCM melting temperature. These locations are displayed in Table 4 and Fig. 3f.

The relative and absolute improvements in electrical output using the PV/PCM cell compared to the reference is shown for the full range of PCM melting temperatures in Fig. 5. At all locations, the improvement in solar PV performance is peaked around the optimal value, however, a PCM melting temperature that is slightly above or below the optimal temperature will still

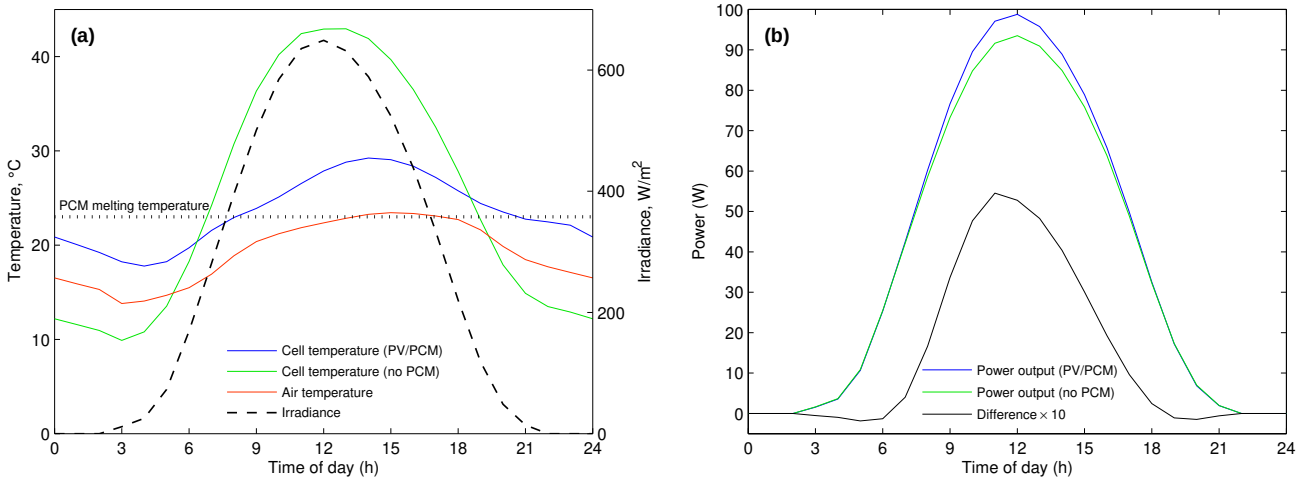

Figure 2: (a) Temperatures of PV/PCM and reference cells. PV cell temperature with a PCM (blue) and without a PCM (green) for a northern hemisphere location in June. Also shown is air temperature (red) and horizontal solar irradiance (black dashes, right scale). The PCM melting temperature is 23°C. (b) Power output from PV/PCM cell and reference cell. Also shown is the power output improvement of PV/PCM cell multiplied by a factor of 10 (black curve).

Name	Country	Location	Size	Reference
Agua Caliente	USA	33.0°N, 113.5°W	250 MW	[27]
Mesquite	USA	33.3°N, 112.9°W	150 MW	[28]
Charanka	India	23.9°N, 71.2°E	214 MW	[29]
Golmud	China	36.4°N, 95.3°E	200 MW	[30]
Neuhardenberg	Germany	52.6°N, 14.2°E	145 MW	[31]
Nzema	Ghana	5–11°N, 0–3°W	155 MW	[32]

Table 4: Characteristics of large solar farms investigated. The precise location of Nzema is not known so the latitude/longitude grid that covers the whole of Ghana has been investigated. The two arrays in the USA are close enough together to be grouped in the same grid cell to the resolution of the model. See also Fig. 3f.

deliver most of the increase in performance available at the optimal value. It can be seen in Fig. 5 that when a PCM melting temperature that is significantly different from the optimal is used, performance improvement does not decline further with any additional excursion from optimal melting temperature and is still positive.

5. Discussion

Overall, areas experiencing high levels of solar irradiance appear to benefit most from PCM cooling. This follows from Eqs. (12) and (13) in which a large solar irradiance input I drives an increase in PV front glass and cell temperatures so efforts to mitigate these temperature rises should lead to increased PV efficiency. The main effect of ambient temperature is to determine the most beneficial PCM melting temperature; a hot climate will require a high PCM melting temperature and a cool climate favours a low PCM melting temperature. For areas with comparable insolations, a cooler climate is still preferable with PCM as the PCM helps to keep cell temperature nearer to the ambient, and if the ambient temperature is lower the baseline efficiency will be higher.

The greatest improvements in PV/PCM cell performance are realised by choosing a PCM that fully melts over the course of the day and fully resolidifies in the evening, making use of the latent heat capacity of the phase change material. Following this, PCM melting temperatures that are too high or too low do not produce the required effect, however, the addition of the PCM as a thermal mass to the solar cell does slow down heating and cooling of the solar cell to the effect that the PV/PCM cell does not get as hot as the reference cell during peak solar hours. It is shown in the variation of T_{melt} in Fig. 5 that using a PCM melting temperature that differs from the ideal temperature by a few degrees also results in a significant improvement in PV energy output performance where at least part of the latent heat capacity of the PCM is used.

The results obtained in terms of relative improvement are slightly lower than those found in the literature for an assessment on the efficiency improvement for outdoor tests on PV/PCM systems, i.e. 6.8% in Pakistan and 3.8% in Ireland [7]. However, as this is a global study where one PCM is used for a full year of meteorological conditions, it is likely that there are many times throughout the year that the PCM is non-optimal, unlike in [7] where the experimental period was 2 weeks; in these experiments, day-to-day conditions are likely to be more

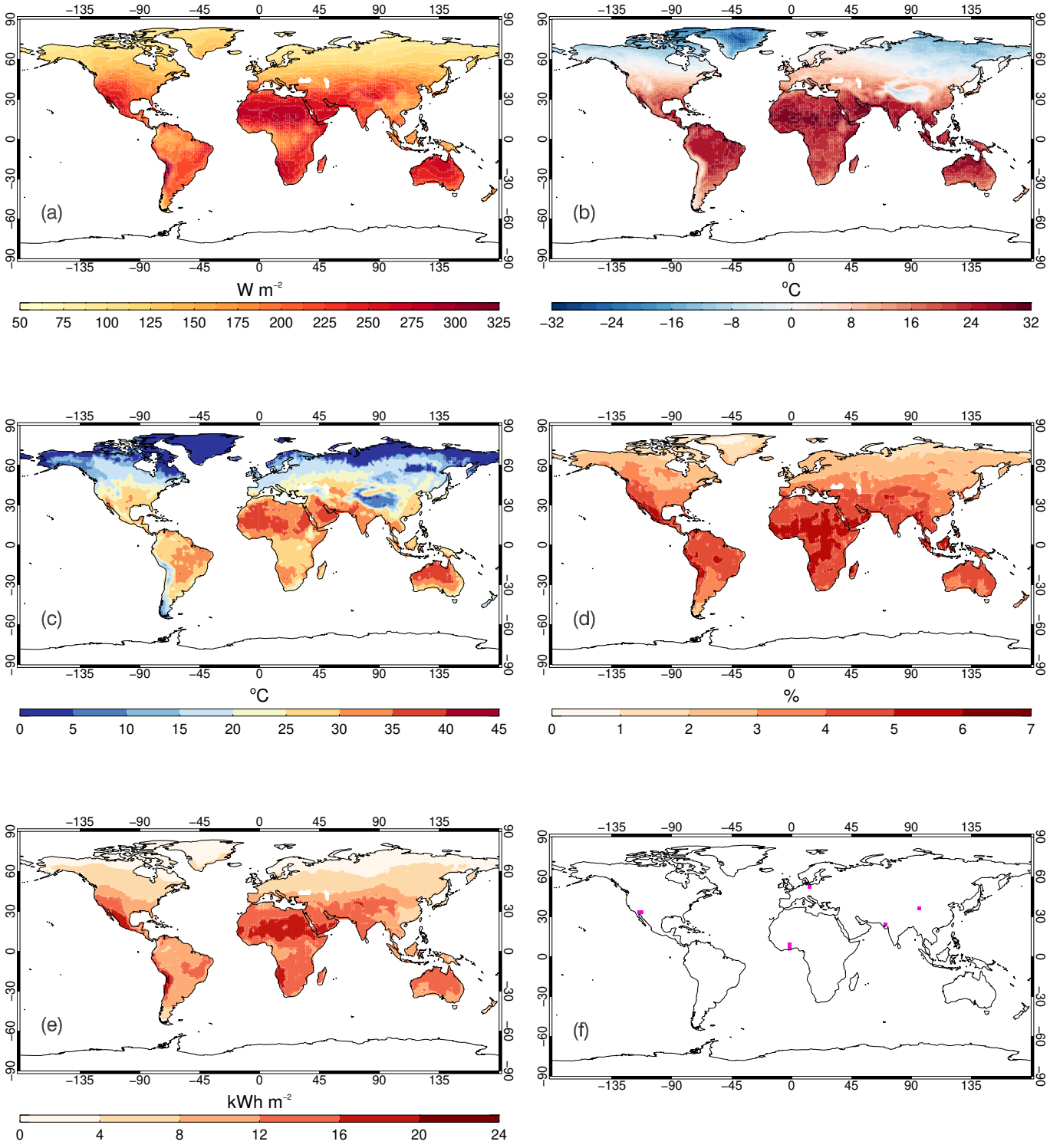

Figure 3: (a) Daily-averaged horizontal insolation for the 12 month period July 2012–June 2013 from the ERA-Interim dataset. (b) Average near-surface air temperature for the July 2012–June 2013 period from ERA-Interim dataset. (c) PCM melting temperature that leads to the greatest increase in solar PV energy output in the PV/PCM system. (d) Increase in electrical output from using the PV/PCM system over the PV reference system with the PCM melting temperature equal to the ideal value from Fig. (c). (e) Total improvement in annual electrical output for a PV/PCM system over the PV reference with the PCM melting temperature equal to the ideal value in Fig. (c). (f) Locations used in the sensitivity analysis (section 4.2).

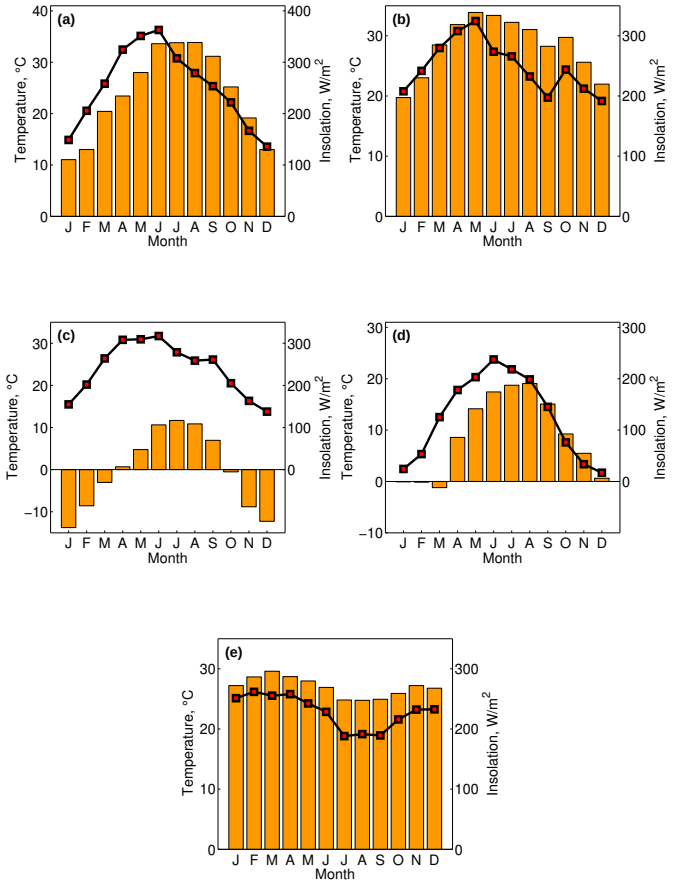

Figure 4: Climate data for the locations analysed in section 4.2: (a) Arizona; (b) India; (c) China; (d) Germany; (e) Ghana. Bars indicate temperature (left scale), lines indicate irradiance (right scale).

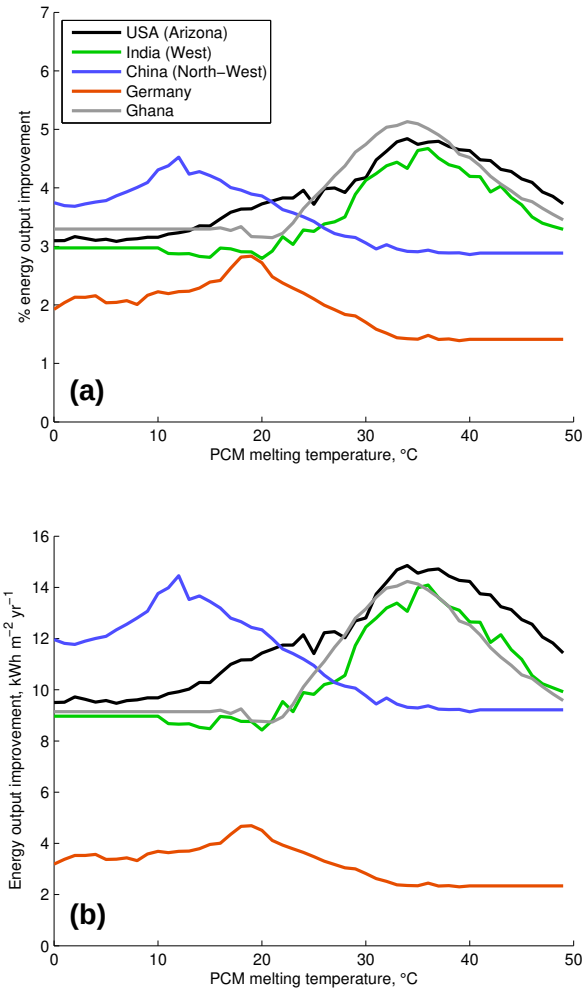

Figure 5: The improvement in PV output as a function of PCM melting temperature T_{melt}.

Commodity	Unit cost	Mass required	Total cost
PCM	€4.93 kg^{-1}	43 kg m^{-2}	€211.99 m^{-2}
Aluminium	€1.60 kg^{-1}	16.2 kg m^{-2}	€32.32 m^{-2}
Total			€244.31 m^{-2}

Table 5: Example costs of materials required to include a 0.05m layer of PCM with aluminium casing. References [34] and [35].

similar and an optimal PCM should perform well across the duration of the experiment. The variability of climate is reflected in the results of this study. Of the locations analysed in detail, Ghana experiences the smallest inter-seasonal variation in temperature and irradiance levels (Fig. 4e). The uniformity of year-round climate means that the annual most beneficial PCM melting temperature is closer to ideal for many months the year which may be why the *relative* increase in electricity output at optimal PCM melting temperature is slightly higher for Ghana than for Arizona, but in absolute terms Arizona produces a bigger improvement. In Germany, where wintertime irradiance is very low, the lowest relative PCM improvement is seen. PCMs may therefore be of limited benefit in areas of low solar irradiance but a PCM that is optimised for summer conditions should perform better than one optimised for the annual mean conditions in higher-latitude locations.

We perform an illustrative cost assessment to determine whether PV/PCM systems would currently be commercially viable. To implement 1 m^{-2} of PV/PCM would require an additional material cost of €244.31 (Table 5). Assuming a 25 year lifespan and typical EU-27 electricity retail costs of €0.1836 kWh^{-1} [33], a PV/PCM system would need to generate an additional 53.2 kWh of electricity per year for each square metre over a PV-only system to overcome these additional material costs. This is not currently satisfied by any location, however this figure would be highly dependent on actual material costs and local energy prices.

6. Conclusions

PV/PCM systems can curb the rapid rise in PV cell temperatures during the daytime and keep PV cell temperatures lower

during the peak solar hours of the day, improving solar cell efficiency and electrical energy output. The input of solar irradiance causes the PV glass and cell to heat up during the daytime. Heat is transferred from the PV cell to the PCM, which acts as a heat sink as it melts, both delaying temperature rise in the PV cell and keeping overall temperature rise lower than in a non-PCM cell. Heat energy is released back from the PCM layer to the solar cell through the evening and overnight.

The benefits of PV/PCM systems at all land locations in the world excluding Antarctica have been demonstrated. Using a numerical finite difference model solving the heat transfer equation, it is shown that energy output improvements over a reference system with no PCM are everywhere positive and in some locations in excess of 6% on an annualised basis, with many regions of the world experiencing a potential total energy gain of 23 kWh m^{-2} based on a reference cell efficiency of 15.6%. The best results are seen where an ideal PCM melting temperature for the location in question is used and the PCM melts fully over the course of the day and resolidifies in the evening. In this case the full latent heat content of the PCM is used and the PCM layer acts as thermal mass with a high effective heat capacity. PV/PCM systems provide the greatest improvements in absolute and relative terms in Africa, South Asia, Australia and South and Central America. These areas receive high levels of irradiance and often experience high ambient temperatures year-round. Many of these are areas where solar energy could greatly aid development by providing an abundant, reliable electricity source. It has been demonstrated that single junction silicon PV/PCM systems are not currently cost-effective, but this may be possible for technologies such as concentrating PV and multi-junction solar cells which reach higher temperatures and electrical outputs. Furthermore, we did not consider tracking systems in our paper, which most utility-scale solar farms would implement. Based on this global overview, more detailed regional models could be explored to further isolate the conditions necessary for enhanced solar PV energy output using phase change materials.

Acknowledgements

This work was financially supported by the Engineering and Physical Sciences Research Council through the University of Leeds Doctoral Training Centre in Low Carbon Technologies.

References

[1] M. J. Huang, P. C. Eames, B. Norton, Thermal regulation of building-integrated photovoltaics using phase change materials, International Journal of Heat and Mass Transfer 47 (12-13) (2004) 2715–2733.

[2] E. Skoplaki, J. A. Palyvos, On the temperature dependence of photovoltaic module electrical performance: A review of efficiency/power correlations, Solar Energy 83 (5) (2009) 614–624.

[3] S. Krauter, Increased electrical yield via water flow over the front of photovoltaic panels, Solar Energy Materials and Solar Cells 82 (1-2) (2004) 131–137.

[4] C. S. Malvi, D. W. Dixon-Hardy, R. Crook, Energy balance model of combined photovoltaic solar-thermal system incorporating phase change material, Solar Energy 85 (7) (2011) 1440–1446.

[5] M. J. Huang, P. C. Eames, B. Norton, Phase change materials for limiting temperature rise in building integrated photovoltaics, Solar Energy 80 (9) (2006) 1121–1130.

[6] M. J. Huang, The effect of using two PCMs on the thermal regulation performance of BIPV systems, Solar Energy Materials and Solar Cells 95 (3) (2011) 957–963.

[7] A. Hassan, Phase Change Materials for Thermal Regulation of Building Integrated Photovoltaics, Ph.D. thesis, Dublin Institute of Technology, 2010.

[8] S. Maiti, S. Banerjee, K. Vyas, P. Patel, P. K. Ghosh, Self regulation of photovoltaic module temperature in V-trough using a metal-wax composite phase change matrix, Solar Energy 85 (9) (2011) 1805–1816.

[9] S. Armstrong, W. G. Hurley, A thermal model for photovoltaic panels under varying atmospheric conditions, Applied Thermal Engineering 30 (11) (2010) 1488–1495.

[10] A. Hasan, S. McCormack, M. Huang, B. Norton, Evaluation of phase change materials for thermal regulation enhancement of building integrated photovoltaics, Solar Energy 84 (2010) 1601–1612.

[11] B. Zalba, J. M. Marín, L. F. Cabeza, H. Mehling, Review on thermal energy storage with phase change: materials, heat transfer analysis and applications, Applied thermal engineering 23 (3) (2003) 251–283.

[12] A. Heinz, W. Streicher, Application of Phase Change Materials and PCM slurries for thermal energy storage, in: Ecostock Conference, Pomona, USA, 2006.

[13] P. Lamberg, R. Lehtiniemi, A. Henell, Numerical and experimental investigation of melting and freezing processes in phase change material storage, International Journal of Thermal Sciences 43 (3) (2004) 277–287.

[14] L. Fan, J. M. Khodadadi, Thermal conductivity enhancement of phase change materials for thermal energy storage: A review, Renewable and Sustainable Energy Reviews 15 (1) (2011) 24–46.

[15] R. Velraj, R. V. Seeniraj, B. Hafner, C. Faber, K. Schwarzer, Heat transfer enhancement in a latent heat storage system, Solar Energy 65 (3) (1999) 171–180.

[16] O. Öttinger, PCM/Graphitverbund-Produkte für Hochleistungswärmespeicher, in: ZAE Symposium: Wärme- und Kältespeicherung mit Phasenwechselmaterialien (PCM), 2004.

[17] M. Zukowski, Mathematical modeling and numerical simulation of a short term thermal energy storage system using phase change material for heating applications, Energy Conversion and Management 48 (2007) 155–165.

[18] P. W. Bridgman, A complete collection of thermodynamic formulas, Physical Review 3 (1914) 273–281.

[19] European Centre for Medium-range Weather Forecasting, ERA Interim, Synoptic Monthly Means, Full Resolution. Available from `http://data-portal.ecmwf.int/data/d/interim_full_mnth/`. Last accessed 20 September 2013.

[20] D. Dee, S. Uppala, A. Simmons, P. Berrisford, P. Poli, S. Kobayashi, U. Andrae, M. Balmaseda, G. Balsamo, P. Bauer, P. Bechtold, A. Beljaars, L. van de Berg, J. Bidlot, N. Bormann, C. Delsol, R. Dragani, M. Fuentes, A. Geer, L. Haimberger, S. Healy, H. Hersbach, E. Hólm, L. Isaksen, P. Kållberg, M. Köhlera, M. Matricardi, A. McNally, B. Monge-Sanz, J.-J. M. abd B.-K. Park, C. Peubey, P. de Rosnay, C. Tavolato, J.-N. Thépauta, F. Vitarta, The ERA-Interim reanalysis: configuration and performance of the data assimilation system, Quarterly Journal of the Royal Meteorological Society 137 (2011) 553–597.

[21] G. Notton, C. Cristofari, M. Mattei, P. Poggi, Modelling of a double-glass photovoltaic module using finite differences, Applied Thermal Engineering 25 (17) (2005) 2854–2877.

[22] W. C. Swinbank, Long-wave radiation from clear skies, Quarterly journal of the Royal Meterological Society 89 (1963) 339–348.

[23] D. L. Loveday, A. H. Taki, Convective heat transfer coefficients at a plane surface on a full-scale building facade, International Journal of Heat and Mass Transfer 39 (8) (1996) 1729–1742.

[24] D. L. Evans, Simplified method for predicting photovoltaic array output, Solar Energy 27 (6) (1981) 555–560.

[25] A. D. Jones, C. P. Underwood, A thermal model for photovoltaic systems, Solar Energy 70 (2001) 349–359.

[26] E. Lorenzo, Energy collected and delivered by PV modules, in: A. Luque, S. Hegedus (Eds.), Handbook of photovoltaic science and engineering, John Wiley and Sons, 905–970, 2003.

[27] First Solar, World's Largest Operational Solar PV Project, Agua Caliente, Achieves 250 Megawatts of Grid-Connected Power. Available from http://investor.firstsolar.com/releasedetail.cfm?ReleaseID=706034. Accessed 4 March 2013.

[28] Energy Matters, Construction Of Mesquite Solar 1 Completed. Available from http://www.energymatters.com.au/index.php?main_page=news_article&article_id=3545. Accessed 4 March 2013.

[29] S. McMahon, Gujarat's 214MW solar park named as Asia's largest single PV plant. Available from http://www.pv-tech.org/news/gujarats_214mw_solar_park_named_as_asias_largest_single_pv_plant.

[30] A. Cohen, Solar Farms. Available from http://www.thehouseofsolar.com/solar-farms/. Accessed 4 March 2013.

[31] D. Lenardic, Large-scale photovoltaic power plants ranking 1–50. Available from http://www.pvresources.com/PVPowerPlants/Top50.aspx. Accessed 4 March 2013.

[32] C. Rhead, Africa's largest solar PV plant. Available from http://www.blue-energyco.com/news/africas-largest-solar-pv-plant/. Accessed 4 March 2013.

[33] European Commission, EU energy in figures – pocketbook 2012. Available from http://ec.europa.eu/energy/publications/doc/2012_energy_figures.pdf. Last accessed 20 February 2014.

[34] A. López-Navarro, J. Biosca-Taronger, J. Corberán, C. P. nalosa, A. Lázaro, P. Dolado, J. Payá, Performance characterization of a PCM storage tank, Applied Energy 119 (2014) 151–162.

[35] Alibaba, Aluminium sheet products. Available from http://www.alibaba.com/showroom/aluminum-sheet.html. Accessed 21 February 2014.